Subtleties of arithmetical quantum chaos

R. Aurich, F. Scheffler, and F. Steiner
II. Institut für Theoretische Physik, Universität Hamburg, Luruper Chaussee 149, 22761 Hamburg, Germany
(Received 6 September 1994; revised manuscript received 21 November 1994)

The spectral statistics of two closely related strongly chaotic quantum billiards are studied. Both are defined on the same triangular domain on the hyperbolic plane and differ only in the choice of the boundary conditions on the edges of the billiards. The fundamental domain is generated by the action of the reflection group $T^*(2,3,8)$, which is an arithmetical group leading to an exponentially degenerate length spectrum of the classical periodic orbits. The boundary conditions on one billiard, called billiard $\mathcal{A}$, are chosen such that it does not belong to a representation of the reflection group, whereas for billiard $\mathcal{B}$ the boundary conditions correspond to an irreducible symmetry representation. The crucial property of arithmetical chaos, i.e., the exponential degeneracy of periodic orbits having the same length, is not affected by the choice of the boundary conditions. For both billiards our analysis of the spectral statistics is based on the first 1050 quantal energy levels, which we have computed using the boundary element method. It is found that the quantal level statistics for billiard $\mathcal{B}$ show the peculiar properties typical for arithmetical quantum chaos, as discovered previously for other arithmetical systems. Billiard $\mathcal{A}$, however, behaves generically in that it shows at short- and medium-range correlations a behavior in agreement with the random-matrix theory. The periodic-orbit theory is scrutinized to shed some light on the mysterious differences between these two almost identical quantum billiards. The trace of the cosine-modulated heat kernel and the spectral form factor are studied. It is demonstrated that subtle properties of the characters attached to the classical periodic orbits are very important ingredients in the phenomenon of arithmetical quantum chaos.

PACS number(s): 05.45.+b, 03.65.−w

I. INTRODUCTION

This paper is devoted to a study of the energy level statistics of quantum systems whose classical counterparts are strongly chaotic. Special emphasis is put on the so-called arithmetical chaos and the peculiarities of the quantum spectrum ascribed to the exponential degeneracy of the length spectrum of the periodic orbits of the classical counterpart.

General wisdom holds that the statistical properties of quantum levels of chaotic systems are in accordance with random-matrix theory [1]. Lacking any analytical proof that random-matrix theory is applicable to quantum chaotic systems, one is doomed to carry out numerical studies. Up to now only the periodic-orbit theory [2] has provided access to a satisfactory description of the energy spectra. The predictions of random-matrix theory were first tested for the Sinai billiard [3] and the stadium billiard [4], where the level spacing statistic $P(s)$ and the spectral rigidity $\Delta_3(L)$ were studied. Meanwhile, there are many chaotic systems for which the energy spectra have been computed and compared with the predictions of random-matrix theory [2]. However, the investigations are, in most cases, restricted to the short- and medium-range correlations in the energy spectra, which seem to confirm the agreement with random-matrix theory. The long-range correlations do not show a universal behavior since they are determined by the short periodic orbits that depend sensitively on the given system. According to a model [5] based on the periodic-orbit theory, the short-range correlations, in contrast, are determined by the long periodic orbits whose lengths show no sensitive dependence on the given system since they are lying exponentially dense near each other. The mean difference between neighboring lengths is determined by the exponential proliferation of the number $N(l)$ of periodic orbits with lengths shorter than l, which is asymptotically given by $N(l) \sim \frac{e^{\tau l}}{\tau l}$, $l \to \infty$, τ being the topological entropy. The exponentially dense lying periodic orbits then blur the individual properties of a given system.

Thus the applicability of random-matrix theory to quantum chaotic systems has to be restricted to the short- and medium-range correlations that are probed by the level spacing $P(s)$ or the number variance $\Sigma^2(L)$ and the spectral rigidity $\Delta_3(L)$ for small values of L. For large L values, the individual properties are measured. This is valid for quantum systems that do not belong to the class of *arithmetical* quantum chaotic systems. In the latter class not even the short-range correlations are in accordance with random-matrix theory, apart from the limit $L \to 0$, which is universal for both chaotic and integrable systems.

The first arithmetical quantum chaotic system for which the deviation from the random-matrix theory expectation was observed was a *triangular billiard* with Dirichlet boundary conditions that tessellates the hyperbolic plane [6]. It is denoted by $T^*(2,3,8)$ because it is characterized by the three angles $\frac{\pi}{2}$, $\frac{\pi}{3}$, and $\frac{\pi}{8}$ (see Fig. 1). The star denotes that the triangle group is actually a reflection group, which needs the complex conjugation in its representation on the Poincaré disk. However, in

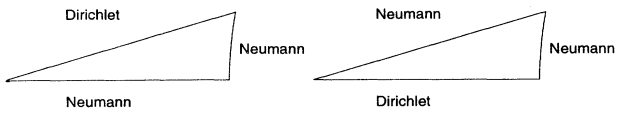

FIG. 1. The quantum billiards $\mathcal{A}$ and $\mathcal{B}$ in the Poincaré disk $\mathcal{D}$. The left triangle defines billiard $\mathcal{A}$ with Neumann boundary conditions on sides a and b and a Dirichlet boundary condition on side c. The right triangle shows billiard $\mathcal{B}$ with a Dirichlet boundary condition on side a and Neumann boundary conditions on sides b and c. The left corners of the triangles are at the origin $z = 0$ of the Poincaré disk $\mathcal{D}$ whose boundary $|z| = 1$ is not shown.

the first studies, the arithmetical property was not acknowledged and the peculiar behavior was attributed to the fact that this billiard tessellates the whole hyperbolic plane. Later studies demonstrated [7] that the energy spectra of nonarithmetical (asymmetric) hyperbolic octagons, which also tessellate the hyperbolic plane, behave in accordance with random-matrix theory with respect to short- and medium-range correlations. This proved that the tessellation argument was not justified.

One was led to the special triangular billiard $\mathrm{T}^*(2,3,8)$ by the study of the geodesic flow on compact Riemann surfaces, represented on the hyperbolic plane, which is considered the prototypical example of a strongly chaotic system. A special Riemann surface of genus $g = 2$, the so-called *regular octagon* [8], was investigated, but because of its high symmetry it has to be desymmetrized. One of its 96 irreducible symmetry representations corresponds to this special triangular billiard.

The central characteristic of arithmetical chaotic systems was discovered at first [9] in the case of the regular octagon for which the length spectrum of periodic orbits was found to be degenerate exponentially with increasing length l according to the mean behavior $\langle g(l) \rangle \sim \rho \frac{e^{l/2}}{l}$, $l \to \infty$, with $\rho = 8\sqrt{2}$ [9]. This exponential degeneracy of the lengths of periodic orbits was rigorously proven for the regular octagon in [10] and for general arithmetical systems in [11,12]. A further arithmetical billiard, which played an important role in the understanding of the behavior of arithmetical quantum systems, is Artin's billiard $\mathrm{T}^*(2,3,\infty)$ [13–16].

In this paper we study the spectral statistics of two triangular quantum billiards, called $\mathcal{A}$ and $\mathcal{B}$, defined on the above mentioned hyperbolic triangle generated by the action of the reflection group $\mathrm{T}^*(2,3,8)$. In the next section we describe in more detail the two quantum billiards $\mathcal{A}$ and $\mathcal{B}$. Section III discusses the statistical properties of the quantal energy spectra with special emphasis on the differences between arithmetical and generic chaos. In Sec. IV the periodic-orbit theory is employed to extract information about the periodic orbits from the quantal energies using the trace of the cosine-modulated heat kernel and the spectral form factor. It is demonstrated that subtle properties of the characters attached to the classical periodic orbits are a very important ingredient in the phenomenon of arithmetical quantum chaos. Section V gives a summary and discussion of the results.

II. THE TRIANGULAR QUANTUM BILLIARDS $\mathcal{A}$ AND $\mathcal{B}$

In this section we shall describe in more detail the two triangular quantum billiards $\mathcal{A}$ and $\mathcal{B}$. Their fundamental domains are classically identical to that of the previously studied billiard $\mathrm{T}^*(2,3,8)$ with Dirichlet boundary conditions. They differ from that triangle only in the chosen boundary conditions. Instead of pure Dirichlet boundary conditions, a mixture of Dirichlet and Neumann boundary conditions is imposed. The classical dynamics is not affected by the chosen boundary conditions, i.e., the classical length spectra of periodic orbits are in all cases identical with respect to the lengths and the degeneracies of the lengths. From the point of view of periodic-orbit theory, the boundary conditions are only reflected by phase factors (characters) in the amplitudes of the periodic-orbit contributions. Choosing on the three sides all possible combinations of Dirichlet and Neumann boundary conditions yields eight different quantum systems. In [17] all eight possible boundary combinations were studied. Based on the first 200 eigenvalues computed by the finite-element method, the energy statistics were shown to be not identical for the eight systems. Four of the eight spectra behaved in accordance with random-matrix theory with respect to short- and medium-range correlations, whereas the other four showed the peculiar behavior typical for arithmetical quantum chaotic systems. It is important to emphasize that all eight billiards possess the same length spectrum, i.e., the lengths as well as the degeneracies are identical. Thus the peculiarities must be due to a much more subtle origin than due to the degeneracies of the lengths.

Let us now discuss the billiards in more detail. They are conservative Hamiltonian systems with two degrees of freedom that classically consist of a point particle sliding freely inside a compact hyperbolic triangle $\mathcal{T}$ with elastic reflections on the boundary $\partial\mathcal{T}$. The Poincaré disk $\mathcal{D}$ is chosen as a model of the hyperbolic surface, which consists of the interior of the unit circle in the complex z plane ($z = x_1 + ix_2$) endowed with the hyperbolic metric

$$g_{ij} = \frac{4}{(1 - x_1^2 - x_2^2)^2}\delta_{ij}, \qquad i,j = 1,2 \tag{1}$$

corresponding to constant negative Gaussian curvature $K = -1$. This fixes the length scale.

The classical motion (geodesic flow) is determined by the Hamiltonian $H = \frac{1}{2m}p_i g^{ij} p_j$, $p_i = m\, g_{ij}\, dx^j/dt$. The classical trajectories consist of geodesic pieces where the geodesics are circles intersecting the boundary of the Poincaré disk $\mathcal{D}$ perpendicularly.

The quantum mechanical system is governed by the Schrödinger equation ($z \in \mathcal{T}$)

$$-\Delta\Psi_n(z) = E_n\Psi_n(z) \quad ,$$

$$\Delta = \frac{1}{4}(1 - x_1^2 - x_2^2)^2 \left(\frac{\partial^2}{\partial x_1^2} + \frac{\partial^2}{\partial x_2^2}\right) \quad , \tag{2}$$

where Δ denotes the non-Euclidean Laplacian corre-

sponding to the hyperbolic metric (1). Here and in the following units $\hbar = 2m = 1$ are used. The wave functions $\Psi_n(z)$ have to obey proper boundary conditions on the boundary $\partial\mathcal{T}$ of the triangular billiard $\mathcal{T}$.

The hyperbolic triangle $\mathcal{T}$ is defined by the three angles $\alpha = \frac{\pi}{3}$, $\beta = \frac{\pi}{8}$, and $\gamma = \frac{\pi}{2}$ (see Fig. 1). Since the length scale is fixed ($K = -1$), the hyperbolic length a of side a is given by

$$\cosh a = \frac{\cos\alpha + \cos\beta\cos\gamma}{\sin\beta\sin\gamma} , \tag{3}$$

with analogous equations for sides b and c. One has $a = 0.764\,285\ldots$, $b = 0.363\,519\ldots$, and $c = 0.860\,706\ldots$. The area is given by $\text{area}(\mathcal{T}) = \pi/24$.

The triangular billiard tessellates the Poincaré disk $\mathcal{D}$ by the action of the reflection group $\mathrm{T}^*(2,3,8)$, which is generated by the three reflections along the three sides of the triangle. A close inspection of the action of the reflection group on the triangle reveals that sides b and c are mapped onto copies of each other, whereas side a is only mapped onto copies of itself. The consequence is that only those combinations of boundary conditions having the same boundary condition along sides b and c are compatible with the reflection group, i.e., they correspond to a representation of the reflection group, whereas the choice of the boundary condition on side a is not restricted. Thus four combinations are obtained that belong to a representation of the reflection group and four that do not, but all the eight classical systems nevertheless tessellate the whole Poincaré disk $\mathcal{D}$. It has been pointed out in [17] that the four triangular billiards that yield subspectra of the spectrum of the regular octagon and are thus compatible with the reflection group show the peculiar behavior characteristic for arithmetical chaos, while the other four behave according to random-matrix theory at small- and medium-range correlations. It is worthwhile to note that Gutzwiller's semiclassical periodic-orbit theory [2] is only exact for the compatible case since only in that case one can derive the trace formula without any approximation, as Selberg has shown for general Fuchsian groups [18].

We choose the following two combinations of boundary conditions: For the incompatible case we choose Neumann boundary conditions on sides a and b and a Dirichlet boundary condition on side c. In the following this quantum billiard is called billiard $\mathcal{A}$. The other billiard, which we call billiard $\mathcal{B}$, is defined by a Dirichlet condition on side a and Neumann conditions on sides b and c. The quantum billiard $\mathcal{B}$ represents the compatible case that corresponds to a representation of the reflection group. Both billiards are illustrated in Fig. 1. We would like to emphasize that billiard $\mathcal{A}$ and billiard $\mathcal{B}$ possess the same arithmetical structure leading to the same length spectrum of periodic orbits. Using the boundary element method [19] we have computed all quantal energies $0 < E_1 \le E_2 \le \cdots$ up to $E = 100\,000$, containing roughly 1050 levels for each billiard. The ground-state energies are $E_1 = 45.58$ for billiard $\mathcal{A}$, and $E_1 = 32.67$ for billiard $\mathcal{B}$. We observe no degeneracies among the computed quantal levels.

III. LEVEL STATISTICS

A. The Weyl series

The first step in the analysis of the statistical properties of the quantal levels of billiard $\mathcal{A}$ and billiard $\mathcal{B}$, respectively, is the unfolding of their energy spectra. The quantal energies E_n are mapped by

$$x_n = \overline{\mathcal{N}}(E_n) \tag{4}$$

onto a normalized spectrum $\{x_n\}$ having a mean level spacing of unity. Here $\overline{\mathcal{N}}(E)$ denotes the Weyl series that describes the asymptotic behavior of the spectral staircase $\mathcal{N}(E)$ counting the quantal levels up to energy E

$$\overline{\mathcal{N}}(E) = \frac{\text{area}(\mathcal{T})}{4\pi} E + \frac{\varepsilon^a a + \varepsilon^b b + \varepsilon^c c}{4\pi} \sqrt{E} + \sigma , \tag{5}$$

where $\text{area}(\mathcal{T}) = \pi/24$ denotes the area of the triangle and a, b, and c are the hyperbolic lengths of the corresponding sides [see Eq. (3)]. The boundary conditions

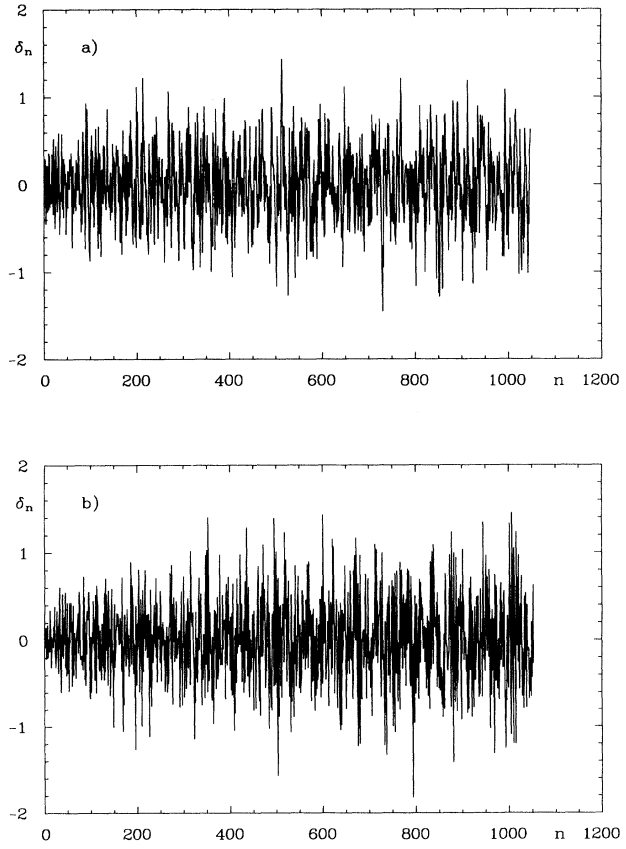

FIG. 2. The spectral fluctuations δ_n are shown for (a) billiard $\mathcal{A}$ and (b) billiard $\mathcal{B}$.

determine ε^i to be $+1$ for a Neumann boundary condition and -1 for a Dirichlet condition. The constant σ is obtained from a fit to the energy spectra yielding -0.188 for billiard $\mathcal{A}$ and -0.125 for billiard $\mathcal{B}$. (See also the discussion at the end of Sec. IV A.) In Fig. 2 the spectral fluctuations

$$\delta_n := x_n - (n - \tfrac{1}{2}) \quad , \quad n = 1, 2, 3, \ldots \tag{6}$$

are plotted for both billiards. In both cases one observes fluctuations around zero, which illustrates that the Weyl series (5) describes indeed the mean behavior of the smoothed counting function $\mathcal{N}(E)$. In addition, this shows that there are no missing levels in the computed spectra.

B. The level spacing statistic $P(s)$

One of the simplest statistics is the level spacing statistic $P(s)$, which describes the distribution of the spacings $s_n = x_{n+1} - x_n$ of adjacent quantal levels. Since the billiards are invariant under time reversal, one has to compare the energy statistics with the Gaussian orthogonal ensemble (GOE) of random-matrix theory [1]. The GOE level spacing is well approximated by Wigner's surmise

$$P_{\mathrm{GOE}}(s) \simeq \frac{\pi}{2} s e^{-\frac{\pi}{4}s^2}, \tag{7}$$

showing a linear level repulsion for $s \to 0$ that is typical for quantum chaotic systems with time-reversal symmetry. In contrast, integrable systems are expected to possess Poisson distributed quantal levels whose level spacing is given by

$$P_{\mathrm{Poisson}}(s) = e^{-s}, \tag{8}$$

which is maximal for $s = 0$ and thus shows level attraction in striking contrast to the GOE case. The level spacings $P(s)$ are displayed in Fig. 3. The level spacing for billiard $\mathcal{A}$ containing all levels up to $E = 100\,000$ is shown in Fig. 3(a) in comparison with Wigner's surmise (7) and very good agreement is observed. Figure 3(b) shows $P(s)$ for billiard $\mathcal{B}$, again using all levels up to $E = 100\,000$ in comparison with the Poisson level spacing (8). In this case the level spacing does not reveal any indication of level repulsion and clearly violates the GOE behavior. It is impressive to see the striking difference between the two cases since only a slight alteration of the boundary conditions, i.e., the interchange of the boundary conditions on sides a and c, distinguishes these otherwise identical billiards. But notice that billiard $\mathcal{B}$ does not show agreement with the Poisson expectation. Nevertheless, it may be that the Poisson behavior is reached in the semiclassical limit $E \to \infty$. This is indeed the case for Artin's billiard, another arithmetical billiard, for which $P(s)$ has been computed in two energy ranges in [14]. There it is observed that $P(s)$ approaches, in the low-energy range at $s = 0$, a value of roughly 0.6, similar to our case. In addition, in [14] $P(s)$ is shown for a very high-energy range, where good agreement with the Poisson curve is observed. To test the possibility that billiard

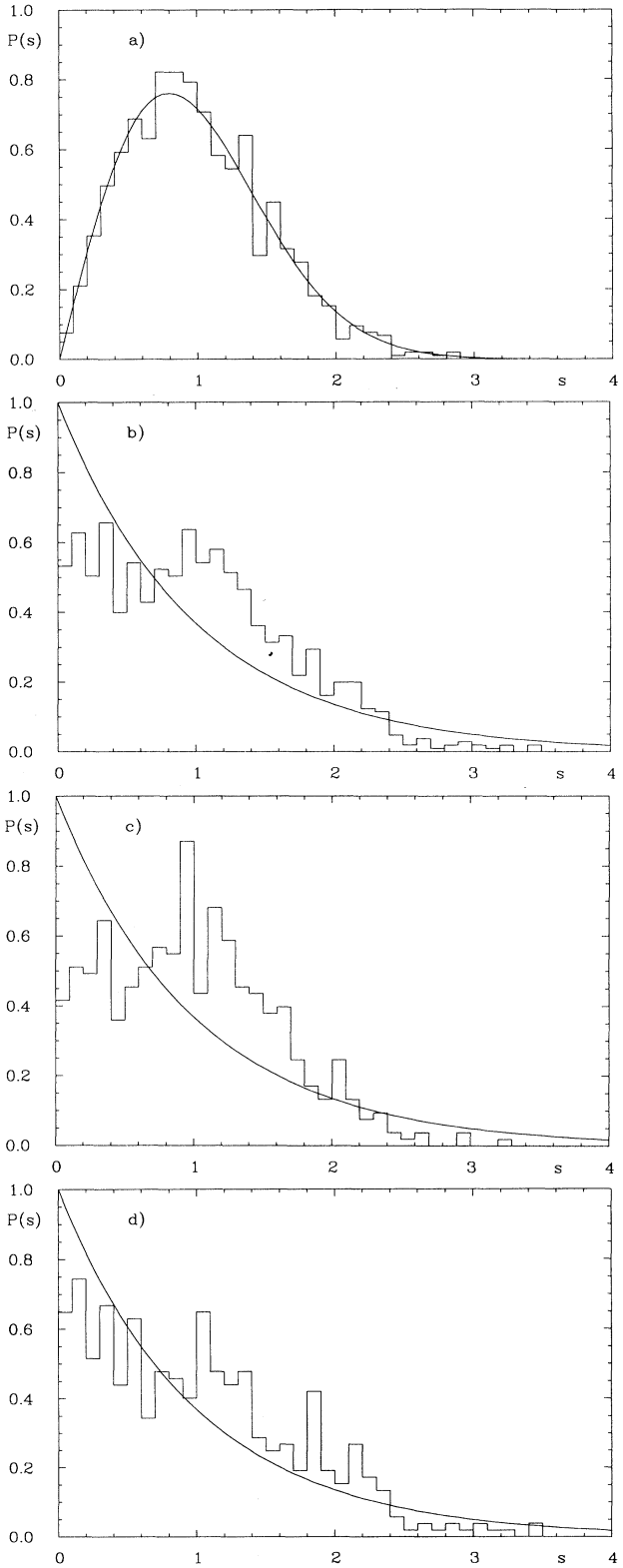

FIG. 3. The level spacing $P(s)$ is displayed for billiard $\mathcal{A}$ in comparison with Wigner's surmise (7) (a) for all energies $E_n < 100\,000$, (b)–(d) $P(s)$ for billiard $\mathcal{B}$ for the energy ranges (b) $E_n \in [0, 100\,000]$, (c) $E_n \in [0, 50\,000]$, and (d) $E_n \in [50\,000, 100\,000]$. The smooth curve in (b)–(d) represents the Poisson expectation (8).

$\mathcal{B}$ behaves in an analogous way, we split the energy interval into $E \in [0, 50\,000]$ and $E \in [50\,000, 100\,000]$. The result is shown in Figs. 3(c) and 3(d). The distribution indeed tends at higher energies more to the Poisson curve and at $s = 0$ the distribution increases roughly from 0.4 to 0.7. The numerical results thus may be interpreted to indicate that the level spacing of billiard $\mathcal{B}$ approaches a Poisson distribution in the semiclassical limit. If this were indeed the case, there arises the interesting question of why the semiclassical limit is reached so slowly in comparison to billiard $\mathcal{A}$, for which the GOE curve is already a satisfactory description in the low-energy range; this has often been observed for other systems and, as an example, we would like to recall the results in the case of the asymmetric hyperbolic octagons [7] where the energy statistics were studied for an ensemble of 30 different octagons. A superposition of their spectra with only the first 75 quantal levels already shows a striking agreement with the GOE prediction.

Since the level spacing statistics of arithmetical chaotic systems are not stationary in the commonly accessible energy range comprising the first 1000 levels, another property has been found that distinguishes arithmetical systems from the generic class.

C. The number variance $\Sigma^2(L)$

The number variance allows a convenient inspection of the properties of the energy spectrum over all scales of correlation lengths. In contrast to the nearest-neighbor level spacing $P(s)$, which measures only short correlation lengths, the number variance $\Sigma^2(L)$ probes the spectrum over all correlation lengths L. The number variance describes the fluctuations of the number $n(L)$ of levels contained in a randomly chosen interval of length L and is defined as

$$\Sigma^2(L) := \left\langle (n(L) - L)^2 \right\rangle \quad , \tag{9}$$

where the angular brackets $\langle\,\rangle$ denote a local averaging over sufficiently many levels. In definition (9) it is assumed that the energy spectrum is already unfolded such that $\langle n(L) \rangle = L$. For GOE matrices the random-matrix theory (RMT) yields for the number variance the following exact result:

$$\begin{aligned}\Sigma^2_{\mathrm{GOE}}(L) = \frac{2}{\pi^2} \Big\{ & \ln(2\pi L) + \gamma + 1 \\ & + \frac{1}{2}\mathrm{Si}^2(\pi L) - \frac{\pi}{2}\mathrm{Si}(\pi L) - \cos(2\pi L) \\ & - \mathrm{Ci}(2\pi L) + \pi^2 L \left(1 - \frac{2}{\pi}\mathrm{Si}(2\pi L)\right) \Big\} \,,\end{aligned} \tag{10}$$

where γ denotes Euler's constant. Many quantum chaotic systems show reasonably good agreement with (10) for short- and medium-range correlations. In the large L range they typically display a fluctuating behavior around a plateau, whereas in the GOE case the number variance $\Sigma^2_{\mathrm{GOE}}(L)$ increases logarithmically for $L \to \infty$, as determined by the first term in (10).

Let us now discuss the number variance for the two billiards. We choose a rectangular averaging for the local average $\langle\,\rangle$. In Fig. 4 the number variance is shown for billiard $\mathcal{A}$ (full curve) and billiard $\mathcal{B}$ (dashed curve) in comparison with the GOE expectation and the Poisson behavior given by $\Sigma^2_{\mathrm{Poisson}}(L) = L$. In this evaluation all quantal levels up to $E = 100\,000$ have been used. One observes that billiard $\mathcal{A}$, which already displayed for the level spacing a generic behavior, is in good agreement with the GOE behavior up to roughly $L \simeq 1$–2 and fluctuates thereafter around its saturation plateau

$$\Sigma^2_\infty := \lim_{L\to\infty} \left\langle \Sigma^2(L) \right\rangle_L \quad , \tag{11}$$

where $\langle\,\rangle_L$ denotes an averaging over a sufficiently large L interval. Thus there is only a very small L interval corresponding to short-range correlations where the GOE prediction agrees with the number variance. This small interval of agreement between $\Sigma^2(L)$ and the GOE behavior is responsible for the observed GOE-like nearest-neighbor level spacing $P(s)$, which measures essentially the range $L < 2$. This small range is also the range in which a different behavior is revealed by billiard $\mathcal{B}$, which there matches much better a Poisson behavior. Up to $L \simeq 2$ the number variance of billiard $\mathcal{B}$ lies well above the GOE curve. For larger L values there are again the characteristic fluctuations around a plateau. Thus both billiards show a different behavior only for the short-range correlations, while the medium- and long-range correlations are very similar in both cases. If one studies only the nearest-neighbor level spacings one might be misled to the conclusion that billiard $\mathcal{A}$ shows GOE behavior and billiard $\mathcal{B}$ Poisson behavior. However, this is only true for $L < 2$.

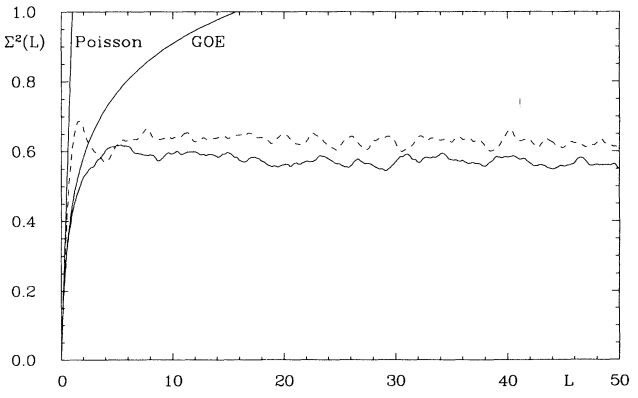

FIG. 4. The number variance $\Sigma^2(L)$ is presented for billiard $\mathcal{A}$ (full curve) and billiard $\mathcal{B}$ (dashed curve) in comparison to the GOE expectation (10) and the Poisson expectation. All quantal levels up to $E = 100\,000$ have been used.

D. The spectral rigidity $\Delta_3(L)$

A similar statistic that has also played a major role in the study of the properties of quantal energy spectra is the spectral rigidity $\Delta_3(L)$ introduced by Dyson and Mehta [20]. The spectral rigidity is defined as the average of the mean square deviation of the staircase $\mathcal{N}(x)$ of the unfolded energy spectrum $\{x_n\} = \{\overline{\mathcal{N}}(E_n)\}$ from the best-fitting straight line $a + b\varepsilon$,

$$\Delta_3(L) := \left\langle \min_{(a,b)} \frac{1}{L} \int_{-L/2}^{L/2} d\varepsilon \, [\mathcal{N}(x+\varepsilon) - a - b\varepsilon]^2 \right\rangle \quad ,$$

$$x := \overline{\mathcal{N}}(E) \quad , \tag{12}$$

where $\langle\,\rangle$ again denotes a local average. The constants a and b can be eliminated, yielding the well-known expression

$$\Delta_3(L) = \left\langle \frac{1}{L} \int_{-L/2}^{L/2} d\varepsilon \mathcal{N}^2(x+\varepsilon) - \left[\frac{1}{L} \int_{-L/2}^{L/2} d\varepsilon \mathcal{N}(x+\varepsilon) \right]^2 - 12 \left[\frac{1}{L^2} \int_{-L/2}^{L/2} d\varepsilon \varepsilon \mathcal{N}(x+\varepsilon) \right]^2 \right\rangle \quad . \tag{13}$$

The spectral rigidity $\Delta_3(L)$ is, in the case of random matrices, closely related to the number variance by the equation

$$\Delta_3^{\mathrm{RMT}}(L) = \frac{2}{L^4} \int_0^L \left(L^3 - 2L^2 r + r^3 \right) \Sigma^2_{\mathrm{RMT}}(r) \, dr \quad . \tag{14}$$

The GOE behavior of the spectral rigidity is determined by Eqs. (10) and (14). Based on Gutzwiller's periodic-orbit theory [2] Berry gives in [5] arguments why the spectral rigidity shows, for energy spectra of chaotic systems, a saturation for $L \gg L_{\max}$ and a behavior consistent with random-matrix theory below $L_{\max}$, where $L_{\max} = 2\pi\bar{d}(E)/T_{\min}$ with $T_{\min}$ being the period of the shortest periodic orbit and $\bar{d}(E)$ the mean level density. Furthermore, it is expected that the saturation value $\Delta_\infty := \lim_{L\to\infty} \Delta_3(L)$ increases logarithmically with increasing energy E. According to the arguments given by Berry [5], for billiards $\mathcal{A}$ and $\mathcal{B}$ one expects the energy dependence

$$\Delta_\infty(E) = \frac{1}{2\pi^2} \ln E + c(l_0) \quad , \tag{15}$$

where the constant is in its crudest approximation given by $c(l_0) = \frac{1}{\pi^2} \ln[4\pi e \bar{d}(E)/l_0] - \frac{1}{8}$ with $l_0 = 0.6330\ldots$ being the length of the shortest periodic orbit. The mean level density $\bar{d}(E)$ is, for two-dimensional billiards, a constant plus nonleading terms and for our billiards it is given by [see Eq. (5)] $\bar{d}(E) = \frac{1}{96} + O(E^{-1/2})$. With these values one obtains $c(l_0) = -0.183\,36\ldots$. For integrable systems one expects instead the semiclassical behavior $\Delta_\infty(E) \sim \sqrt{E}$.

In Fig. 5 the spectral rigidity $\Delta_3(L)$ is shown for billiard $\mathcal{A}$ (full curve) and billiard $\mathcal{B}$ (dashed curve) in comparison with the GOE and Poisson expectations using all quantal levels up to $E = 100\,000$. As in the case of the number variance, one observes, at small correlation lengths $L < 4$, reasonable agreement with the GOE curve for billiard $\mathcal{A}$ and with the Poisson curve for billiard $\mathcal{B}$. The spectral rigidity of billiard $\mathcal{B}$ lies clearly above the GOE curve for $L < 15$ so that a saturation effect cannot be claimed as the cause for the deviation from the GOE curve. The saturation behavior is similar for both billiards, except that the saturation value is slightly larger for billiard $\mathcal{B}$.

Since the spectral rigidity shows a much smoother behavior than the number variance, it is more suited for a study of the energy dependence of the saturation of the energy fluctuations. In Fig. 6 the spectral rigidity is shown for different energy intervals where Fig. 6(a) deals with billiard $\mathcal{A}$ and Fig. 6(b) with billiard $\mathcal{B}$. The available energy range has been split in four intervals of length $\Delta E = 25\,000$, i.e., $E \in [0, 25\,000]$ (full curve), $E \in [25\,000, 50\,000]$ (dotted curve), $E \in [50\,000, 75\,000]$ (dashed curve), and $E \in [75\,000, 100\,000]$ (dash-dotted curve). It is seen that the GOE and the Poisson behavior match, respectively, over an increasing interval with increasing energy until the spectral rigidities drop below the GOE or the Poisson behavior to approach their saturation values. The saturation values show a tendency towards higher values with increasing energy. One observes an exception in the case of billiard $\mathcal{A}$, where the dotted curve belonging to the energy range $[25\,000, 50\,000]$ lies above the dashed curve belonging to $[50\,000, 75\,000]$.

If arithmetical quantum chaotic systems behave more like integrable systems with respect to their spectral statistics, one would expect that the saturation value

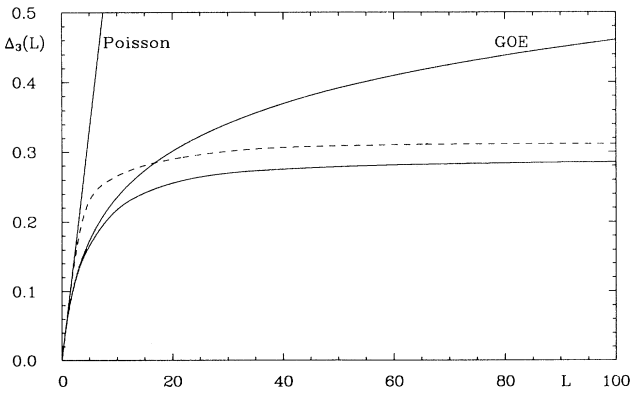

FIG. 5. The spectral rigidity $\Delta_3(L)$ is presented for billiard $\mathcal{A}$ (full curve) and billiard $\mathcal{B}$ (dashed curve) in comparison to the GOE expectation and the Poisson expectation. All quantal levels up to $E = 100\,000$ have been used.

goes like $\Delta_\infty(E) = \alpha\sqrt{E} + \beta$ in the case of billiard $\mathcal{B}$ and like $\Delta_\infty(E) = \frac{1}{2\pi^2}\ln E + \gamma$ in the case of billiard $\mathcal{A}$. To test this hypothesis we computed the saturation values over an energy range $[E_n, E_n + \Delta E]$ with $E_n = 10\,000(n-1)$, $n = 1, 2, \ldots, 8$, and $\Delta E = 30\,000$ yielding eight intervals in the available range $[0, 100\,000]$. The saturation value Δ_∞ itself was determined from a fit of $\Delta_3(L)$ in the range $L \in [15, 50]$ to the function

$$f_\Delta(L) = \Delta_\infty \left(1 + \frac{c_1}{L} + \frac{c_2}{L^2}\right) \quad , \tag{16}$$

where Δ_∞, c_1, and c_2 are the fit parameters. In this way we obtained eight saturation values for each billiard, which in turn allows a fit of $\Delta_\infty(E)$. The fit parameters obtained are $\alpha = 9.7633 \times 10^{-4}$, $\beta = 0.115\,69$, and $\gamma = -0.249\,98$. The results are shown in Fig. 7. The values for billiard $\mathcal{A}$ are shown as full circles in comparison with the logarithmic fit function (full curve), using the above value for γ. The fit is reasonably good. The main deviation occurs for billiard $\mathcal{A}$ at $E = 65\,000$, where the saturation value drops somewhat below the fit. It is the same anomaly that we have already observed in Fig. 6(a). However, over the whole energy range considered, the logarithmic increase is confirmed. The fit constant γ differs from the approximation $c(l_0)$ given below Eq. (15) by a value of 0.066 62. This may appear as a small difference; however, a look at Fig. 7 reveals that the constant $c(l_0)$ would yield too large saturation values.

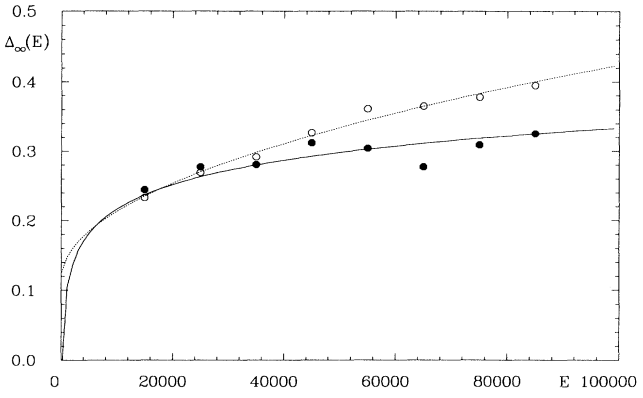

FIG. 7. The energy dependence of the saturation value Δ_∞ of the spectral rigidity is shown. The full dots and the full curve, i.e., the fit result, belong to billiard $\mathcal{A}$, whereas the circles and the dotted curve belong to billiard $\mathcal{B}$.

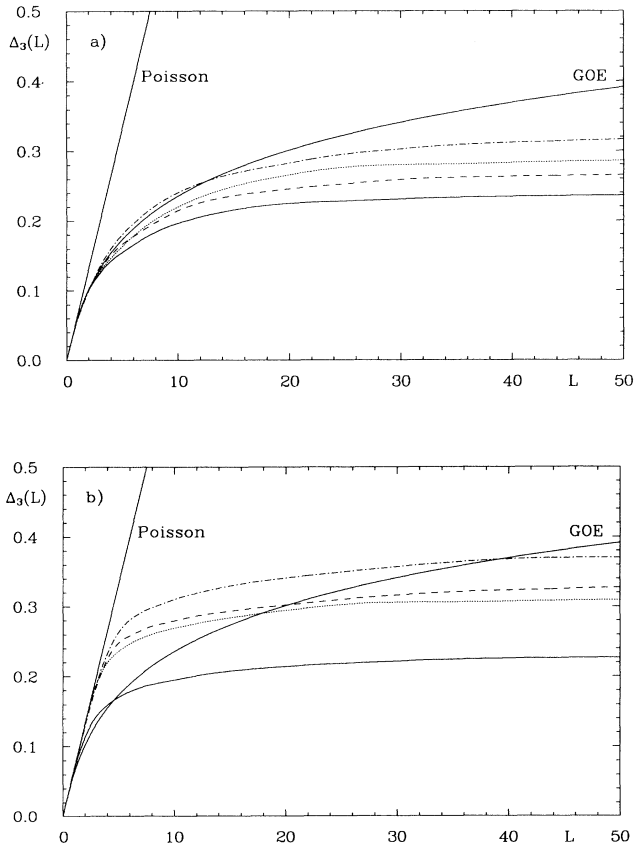

FIG. 6. The energy dependence of the spectral rigidity is shown for (a) billiard $\mathcal{A}$ and (b) billiard $\mathcal{B}$. The four curves correspond to the four energy intervals as explained in the text. In addition the Poisson and the GOE expectation are displayed.

The saturation values $\Delta_\infty(E)$ of the arithmetically behaving billiard $\mathcal{B}$, shown as circles in Fig. 7, are in almost perfect agreement with a "$\sqrt{E}$ behavior" characteristic of integrable systems, which is shown as the dotted curve. A logarithmic behavior seems to be excluded. Arguments based on the diagonal approximation of the spectral form factor lead to a "$\sqrt{E}/\ln E$ behavior" [12], but since this gives an unsatisfactory description of our data, we use in the following the more appropriate $\sqrt{E}$ behavior. A knowledge of the energy dependence of the saturation value of the spectral rigidity is of crucial importance for the mode fluctuation distribution, which we discuss in the following subsection.

E. The mode fluctuation distribution $P(W)$

We have seen in the previous sections that the hypothesis [3,4] that quantum chaotic systems display level fluctuations according to random-matrix theory holds at small- and medium-range correlations only. Thus one has to seek other statistical measures that are able to uncover the "fingerprints" of classical chaos in quantum chaotic systems. To this aim the distribution $P(W)$ of the mode fluctuation $W(E)$ has been proposed in [21,22] as a novel quantity to measure quantum chaos. The (normalized) mode fluctuation $W(E)$ is defined by

$$W(E) := \frac{\mathcal{N}_{\mathrm{fl}}(E)}{\sqrt{\Delta_\infty(E)}} \quad , \tag{17}$$

where $\mathcal{N}_{\mathrm{fl}}(E) := \mathcal{N}(E) - \overline{\mathcal{N}}(E)$ is the fluctuating part

of the mode number $\mathcal{N}(E)$ (spectral staircase function). Since the Weyl series $\overline{\mathcal{N}}(E)$ [see Eq. (5)] describes the mean mode number, it follows that $\mathcal{N}_{\rm fl}(E)$ fluctuates by definition around zero [$\Delta E \gg 1/\bar{d}(E)$]

$$\left\langle \frac{1}{\Delta E} \int_{E-\Delta E/2}^{E+\Delta E/2} dE' \, \mathcal{N}_{\rm fl}(E') \right\rangle \to 0 \ , \quad E \to \infty \ , \tag{18}$$

which in turn implies that the value distribution of $W(E)$, $P(W)$, has zero mean. Furthermore, the second moment of $\mathcal{N}_{\rm fl}(E)$ obeys asymptotically [12]

$$\left\langle \frac{1}{\Delta E} \int_{E-\Delta E/2}^{E+\Delta E/2} dE' \, \mathcal{N}_{\rm fl}^2(E') \right\rangle \sim \Delta_\infty(E) \ , \quad E \to \infty \tag{19}$$

and thus the division by $\sqrt{\Delta_\infty(E)}$ correctly normalizes the distribution of $W(E)$ having unit variance. Since the distribution $P(W)$ has zero mean and unit variance, its specific form is the important measure. In [21,22] the conjecture has been put forth that classically strongly chaotic systems should display, for $E \to \infty$, a universal Gaussian behavior

$$P_{\rm Gauss}(W) = \frac{1}{\sqrt{2\pi}} e^{-\frac{1}{2}W^2} \ , \tag{20}$$

independently of whether the system shows generic or arithmetical chaos, whereas classically integrable systems should reveal themselves by a non-Gaussian distribution $P(W)$. In addition to numerical tests for three different systems, there are further theoretical arguments in support of this hypothesis that have been given in [22]. For some integrable systems, a non-Gaussian distribution has been rigorously proven [23] to hold, whereas the Gaussian is proven to be the exact limit distribution for the nontrivial zeros of the Riemann ζ function using Selberg's moment formalism [24]. The Riemann zeros are interpreted as quantal levels of an unknown quantum chaotic system without time-reversal symmetry. It should be noted that a Gaussian distribution corresponds to maximally random spectra being in agreement with the intuitive prejudice one has on chaotic systems.

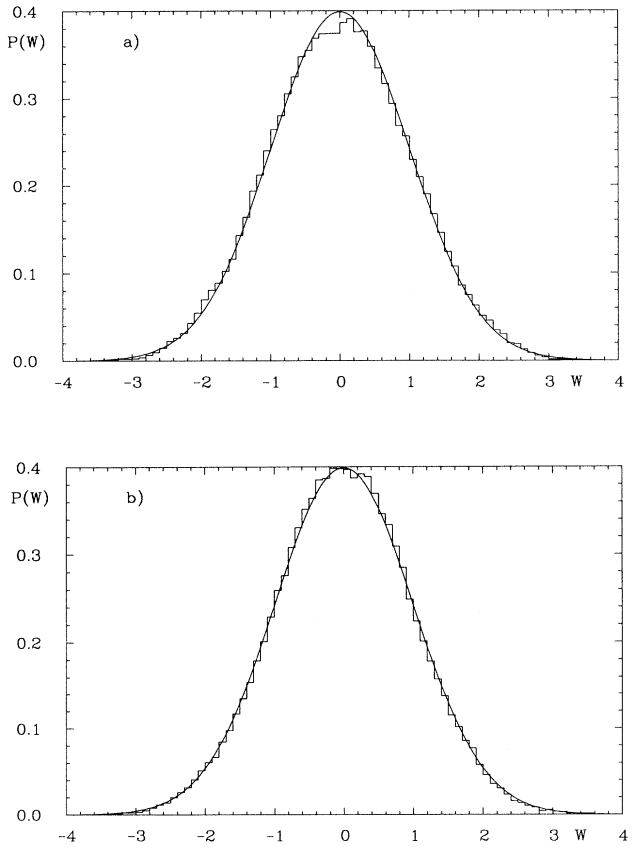

FIG. 8. The mode fluctuation statistic $P(W)$ is shown for (a) billiard $\mathcal{A}$ and (b) billiard $\mathcal{B}$ in comparison with the prediction (20) (full curve).

We have computed the distribution $P(W)$ for both billiards $\mathcal{A}$ and $\mathcal{B}$ using, for $\Delta_\infty(E)$ in the definition (17), the corresponding fits shown in Fig. 7. In Fig. 8(a) the result is shown for the generically behaving billiard $\mathcal{A}$, while Fig. 8(b) presents the results for the arithmetically behaving billiard $\mathcal{B}$. The histograms are computed by evaluating $W(E)$ in steps of $\Delta E = 5$, which gives 20 000 data points up to $E = 100\,000$. The parameter-free expectation (20) is shown as a full curve. The agreement is impressive and underscores the fact that this statistic is universal in that it yields the same distribution for arithmetical and nonarithmetical quantum chaotic systems. We have also applied the Kolmogorov-Smirnov test to the cumulative mode fluctuation distribution testing the cumulative version of the prediction (20). The Kolmogorov-Smirnov test yields the approximate significance level $\mathcal{P}$ of the maximal distance between the cumulative distribution and the theoretical prediction, i.e., $\mathcal{P}$ is the probability to obtain a maximal distance greater than the one observed. For both billiards we obtained high significance levels $\mathcal{P} \gg 1\%$. We get $\mathcal{P} = 23\%$ for billiard $\mathcal{A}$ and $\mathcal{P} = 44\%$ for billiard $\mathcal{B}$. Thus the Kolmogorov-Smirnov test confirms the expectation (20).

IV. PERIODIC-ORBIT THEORY

A. The trace formula

It is most interesting to inquire into the periodic-orbit theory with respect to the level statistics of billiards $\mathcal{A}$ and $\mathcal{B}$. Since both systems have the same classical periodic orbits, i.e., the same lengths and multiplicities, the differences in the level fluctuations over small- and medium-range correlations must be explained by the phase factors attached to the periodic orbits. The starting point is the Selberg trace formula [18] for such billiards. The Selberg trace formula has been specified in

[8] for hyperbolic billiards with identical boundary conditions on all sides, i.e., either only Dirichlet or only Neumann boundary conditions. For the case of mixed boundary conditions compatible with a reflection group Γ, e.g., $\Gamma = \mathrm{T}^*(2,3,8)$, i.e., billiard $\mathcal{B}$ or a billiard with Neumann boundary condition on side a and Dirichlet boundary conditions on sides b and c, the trace formula was derived in [25] and is given by

$$\begin{aligned}\sum_{n=1}^{\infty} h(p_n) = {} & \frac{\mathrm{area}(\mathcal{T})}{4\pi}\int_{-\infty}^{\infty} dp\, h(p)\, p\, \tanh(\pi p) + \sum_{t_{\mathrm{inv}}} \frac{\chi(t)\, l(t)}{4}\, g(0) \\ & + \sum_{t_{\mathrm{ellip}}} \sum_{k=1}^{m_t-1} \frac{\chi^k(t)}{4m_t \sin(\frac{\pi k}{m_t})} \int_{-\infty}^{\infty} dp\, h(p)\, \frac{\exp(-2\pi p \frac{k}{m_t})}{1+\exp(-2\pi p)} \\ & + \sum_{t_{\mathrm{sing}}} \sum_{k=1}^{\infty} \frac{l(t)}{4} \left\{ \frac{\chi^k(t_{\mathrm{even}})}{\sinh[kl(t)/2]} + \frac{\chi(t_{\mathrm{odd}})\,\chi^{k-1}(t_{\mathrm{even}})}{\cosh[kl(t)/2]} \right\} g(kl(t)) \\ & + \sum_{t_{\mathrm{hyp}}} \sum_{k=1}^{\infty} \frac{\chi^k(t)\, l(t)}{\exp[kl(t)/2] - [\sigma(t)]^k \exp[-kl(t)/2]}\, g(kl(t)) \ . \end{aligned} \tag{21}$$

The left-hand side of the trace formula (21) contains the sum over the quantal levels where $p_n = \sqrt{E_n - \frac{1}{4}}$ is the momentum of an eigenstate; it is the quantum mechanical side of the trace formula. The function $h(p)$ is an even test function that is arbitrary, except that it must be holomorphic in a strip $|\,\mathrm{Im}\, p\,| \leq \frac{1}{2} + \varepsilon$, $\varepsilon > 0$, and must decrease faster than $|p|^{-2}$ for $|p| \to \infty$. The Fourier transform of $h(p)$ is denoted by

$$g(x) = \frac{1}{2\pi}\int_{-\infty}^{\infty} dp\, e^{ipx}\, h(p) \ . \tag{22}$$

The right-hand side of (21) is the classical side of the trace formula containing only classical quantities such as the lengths $l(t)$ and the characters $\chi(t)$ corresponding to the elements $t \in \Gamma$. The sum over the conjugacy classes of the reflection group Γ is split according to the special properties of its elements t. The first term on the right-hand side is the so-called zero-length contribution arising from the identity element of Γ. This contribution is also present in Gutzwiller's semiclassical trace formula [2]. The following term is due to the inversion elements t_{inv} of Γ. The next term deals with the elliptic elements $t_{\mathrm{ellip}} \in \Gamma$, where t_{ellip} corresponds to a rotation around $\frac{2\pi}{m_t}$ at a corner point having an angle of $\frac{\pi}{m_t}$. The sum over t_{sing} goes over the singular periodic orbits that are running along the edges of the billiard and deserve a special treatment. Elements t belonging to an even or an odd number of reflections are denoted as t_{even} and t_{odd}, respectively. The last sum over t_{hyp} is the usual periodic orbit contribution also occurring in the generalized trace formula [26], where $\sigma(t) = 1$ for t direct hyperbolic and $\sigma(t) = -1$ for inverse hyperbolic elements $t \in \Gamma$.

The trace formula (21) is an exact relation between quantum and classical mechanics in the case of billiard $\mathcal{B}$, whereas an exact derivation is not possible for billiard $\mathcal{A}$ for which the boundary conditions are not compatible with the reflection group Γ. In this case one is left to use Gutzwiller's semiclassical trace formula. A comparison shows that only the two sums over t_{inv} and t_{ellip} are missing in the standard form of the Gutzwiller trace formula. A further contribution arises from nonperiodic orbits starting and ending in the corner point with angle $\pi/3$. Since in this paper the trace formula is evaluated in terms of the quantal levels, all these terms are included. In the following we shall assume that possible missing terms in the trace formula (21) in the case of billiard $\mathcal{A}$ do not alter our main conclusions. To make this plausible, consider for $h(p)$ the admissible function [27]

$$h(p) = \frac{1}{2}\left\{ \mathrm{erf}\left(\frac{p'-p}{\varepsilon}\right) + \mathrm{erf}\left(\frac{p'+p}{\varepsilon}\right)\right\} \ , \quad \varepsilon > 0 \ , \tag{23}$$

which yields together with (21) the spectral staircase $\mathcal{N}(E)$ in the limit $\varepsilon \to 0$. It is instructive to derive Weyl's law (5) with (23). The area term proportional to E is provided by the zero-length term. Furthermore, this term produces a constant contribution of $-\frac{1}{288}$ to Weyl's law. The perimeter term proportional to $\sqrt{E}$ is generated exactly by the sum over the inversions t_{inv}. An additional constant contribution is eventually produced by the sum over the elliptic elements t_{ellip}. The sums over the periodic orbits, i.e., over t_{sing} and t_{hyp}, yield the oscillatory fluctuations around Weyl's law, which describes only the mean behavior. The first two terms of Weyl's law obtained in this way are identical to the first two terms in (5) for billiard $\mathcal{A}$ as well as for billiard $\mathcal{B}$. For the constant σ one obtains $\sigma = -\frac{73}{576} = -0.1267\ldots$ in the case of billiard $\mathcal{B}$, which is in excellent agreement with our fit value of -0.125 (see Sec. III A). Applying trace formula (21) to billiard $\mathcal{A}$, where it cannot be derived exactly, gives for the constant term $\sigma = -\frac{65}{576} = -0.1128\ldots$, which does not agree so well with our fit value -0.188; nevertheless, the order of magnitude is well matched. This may provide a hint that the unknown corrections are small in this case.

B. The trace of the cosine-modulated heat kernel

The trace of the cosine-modulated heat kernel was introduced in [28,29] to investigate the questions related to "inverse quantum chaology," i.e., the study of the periodic orbits in terms of the quantal levels. (For applications, see [30].) It is obtained from the test function

$$h(p) = \cos(pL)\, e^{-\beta E} \quad , \quad E = p^2 + \frac{1}{4} \quad , \tag{24}$$

whose Fourier transform reads

$$g(x) = \frac{e^{-\beta/4}}{4\sqrt{\pi\beta}} \left\{ e^{-(L-x)^2/4\beta} + e^{-(L+x)^2/4\beta} \right\} \quad , \tag{25}$$

where $\beta > 0$ and $L \in \mathbb{B}$. The Fourier transform (25) has the nice property that it generates, on the right-hand side of the trace formula (21), Gaussian peaks of width $\Delta L \sim 2\sqrt{2\beta}$ exactly at the lengths $l(t)$ of the classical periodic orbits. The peaks are positive or negative depending on the character $\chi(t)$ of the periodic orbit. Thus one can obtain the length spectrum by evaluating the left-hand side using the computed quantal levels.

Let us consider for fixed $\beta > 0$ the following function of L:

$$\Theta^C(L) := \sum_{n=1}^{N} \cos(p_n L)\, e^{-\beta E_n} - \int_0^{p_N} dp\, \cos(pL) e^{-\beta E} \left\{ \frac{p \tanh \pi p}{48} + \frac{1}{4\pi} \sum_{t_{\rm inv}} \chi(t) l(t) \right.$$
$$\left. + \sum_{t_{\rm ellip}} \sum_{k=1}^{m_t - 1} \frac{\chi^k(t)}{4 m_t \sin(\frac{\pi k}{m_t})} \frac{\cosh[\pi p (1 - 2k/m_t)]}{\cosh(\pi p)} \right\} , \tag{26}$$

where we have subtracted from the sum over the computed quantal levels, i.e., the left-hand side of Eq. (21), the zero-length term, the sum over the inversion elements $t_{\rm inv}$, and the sum over the elliptic elements $t_{\rm ellip}$. It follows from the trace formula that $\Theta^C(L)$ is given by the remaining two sums over $t_{\rm sing}$ and $t_{\rm hyp}$ on the right-hand side and thus should show Gaussian peaks at the locations of the various periodic orbits. Ideally, one would like to consider the limit $\beta \to 0$, but since only a finite part $\{E_n\}_{n \le N}$ of the energy spectrum is known, the smallest value of β is determined by the largest computed quantal level, in our case $E_N \simeq 100\,000$, yielding $\beta = 0.000\,05$. Figure 9 presents $\Theta^C(L)$ for billiard $\mathcal{A}$ (full curve) and billiard $\mathcal{B}$ (dotted curve) up to $L = 10$ computed from the first N quantal levels. The first lengths of periodic orbits are well resolved, but with increasing length the length-spacing between neighboring lengths decreases and the peaks soon overlap. The differences between the two curves are due to the different characters $\chi(t)$ for billiards $\mathcal{A}$ and $\mathcal{B}$ determined by the different boundary conditions. The only possibility for further differences is the fact that the trace formula (21) is not exact in the case of billiard $\mathcal{A}$.

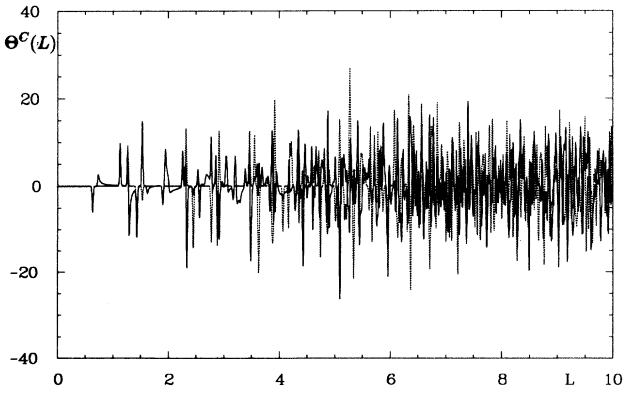

FIG. 9. The trace of the cosine-modulated heat kernel $\Theta^C(L)$ is presented for billiard $\mathcal{A}$ (full curve) and billiard $\mathcal{B}$ (dotted curve) with $\beta = 0.000\,05$ computed from the quantal levels.

The peculiar properties of arithmetical chaos are ascribed to the exponential increase of the mean multiplicities of their length spectra [9,12,14,15]. But the mean multiplicities with respect to the lengths are identical for billiards $\mathcal{A}$ and $\mathcal{B}$ and there arises the delicate question about the origin of the different level statistics for billiards $\mathcal{A}$ and $\mathcal{B}$, as discovered in Sec. III. There is the possibility that in the case of billiard $\mathcal{A}$ the "effective" multiplicity $g_n^{\rm eff} := g_n^+ - g_n^-$ is not exponentially increasing in the sense that for a given length the number of orbits with positive character nearly equals the number of orbits of negative character such that the effective multiplicity $g_n^{\rm eff}$ does not show any exponential behavior. Since it is the effective multiplicity that enters in the spectral form factor, the different spectral behaviors would be explained by this difference. In the case of such a cancellation effect for billiard $\mathcal{A}$, the periodic-orbit theory for this billiard would "see" many fewer periodic orbits and Huber's law for the number of effective periodic orbits would be the standard one, but with a topological entropy of one-half. If such an effect is occurring in billiard $\mathcal{A}$, the trace of the cosine-modulated heat kernel should behave completely differently in both cases. The peaks at the locations of the lengths of periodic orbits

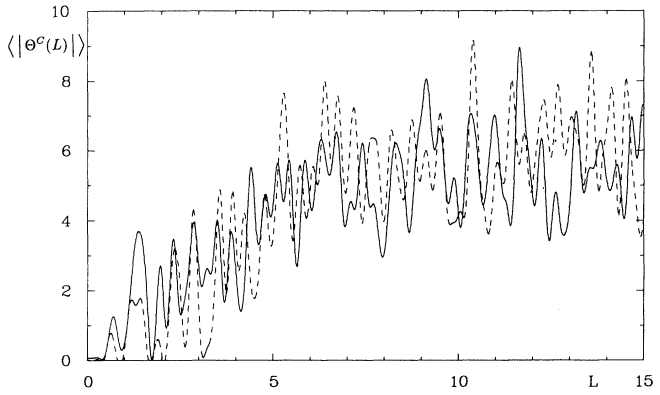

FIG. 10. $\langle\,|\,\Theta^C(L)\,|\,\rangle$ is shown for billiard $\mathcal{A}$ (full curve) and billiard $\mathcal{B}$ (dashed curve).

are proportional to $g_n^{\rm eff}$. Thus one would expect for billiard $\mathcal{A}$ much smaller peaks than for billiard $\mathcal{B}$, where an exponential $g_n^{\rm eff}$ is needed. To test this possibility, we show in Fig. 10 the smoothed average of the modulus of $\Theta^C(L)$, i.e., $\langle\,|\,\Theta^C(L)\,|\,\rangle$, where the full curve belongs to billiard $\mathcal{A}$ and the dashed one to billiard $\mathcal{B}$. Surprisingly, both curves behave very similarly and fluctuate for $L > 5$ around a plateau. Thus our data do not seem to support the idea that a cancellation effect between periodic orbits of the same length occurs in billiard $\mathcal{A}$. One therefore concludes that solely from the exponential increase of the multiplicities one cannot derive Poissonian level fluctuations. Since the periodic-orbit theory should describe the level fluctuations correctly, it seems that the simple models [12,15] considered so far are simplified too much. It appears that a refined model would require more detailed information on the characters and the nonperiodic orbits; the different level statistics for billiards $\mathcal{A}$ and $\mathcal{B}$ must be determined by the subtle differences with respect to their characters and/or the nonperiodic-orbit contributions.

C. The semiclassical spectral form factor

The spectral form factor $K(\tau)$ was introduced in the framework of random-matrix theory for a convenient description of level fluctuations. Defined as $K(\tau) := 1 - b(\tau)$, where $b(\tau)$ is the Fourier transform of the two-level cluster function $Y_2(r)$ [31], it is related to the number variance by the integral transform [20]

$$\Sigma^2(L) = \frac{2}{\pi^2}\int_0^\infty d\tau\,\frac{\sin^2(\pi L\tau)}{\tau^2}\,K(\tau) \quad . \tag{27}$$

The spectral form factor allows a study of the level fluctuations in terms of the periodic orbits. A semiclassical approximation leads to [5]

$$K_{\rm sc}(\tau) = \frac{1}{\bar{d}(\bar{E})}\int_{-\infty}^{\infty} d\varepsilon\;\langle\, d_{\rm fl}(E-\varepsilon/2)\, d_{\rm fl}(E+\varepsilon/2)\,\rangle_{\bar{p},\Delta p} \times\; e^{2\pi i\bar{d}(\bar{E})\varepsilon\tau} \quad , \tag{28}$$

where $\bar{d}(E)$ and $d_{\rm fl}(E)$ are the mean and the fluctuating part of the spectral density $d(E)$, respectively. Expressing $d_{\rm fl}(E)$ by its periodic-orbit expression derived from the trace formula and inserting this into Eq. (28) allows the application of periodic-orbit theory to the study of quantal level statistics. Evaluating the integral in (28) by the method of stationary phase leads to

$$K_{\rm sc}(\tau) = \frac{1}{4\pi\bar{d}(\bar{E})}\left\langle \sum_t \sum_{k=-\infty}^{\infty}{}' \sum_{t'} \sum_{k'=-\infty}^{\infty}{}' \times \frac{A(t,k)\,A^\star(t',k')}{p} e^{ip[kl(t)-k'l(t')]} \times\; \delta\left(\ell - \frac{1}{2}[kl(t)+k'l(t')]\right)\right\rangle_{\bar{p},\Delta p} \quad , \tag{29}$$

where the amplitudes $A(t,k)$ of the periodic orbits can be read off from the trace formula (21) and

$$\ell := 4\pi p\bar{d}(E)\,\tau \quad . \tag{30}$$

The prime at the k sum counting positive and negative traversals denotes that $k = 0$ is excluded. Assuming for the average $\langle\,\rangle$ a Gaussian average around the momentum $\bar{p}$ with width Δp,

$$\langle f(p)\rangle_{\bar{p},\Delta p} := \int_{-\infty}^{\infty} dp\,\frac{1}{\sqrt{2\pi}\Delta p}\,e^{-\frac{(p-\bar{p})^2}{2\Delta p^2}}\,f(p) \quad , \tag{31}$$

one obtains

$$K_{\rm sc}(\tau) = \frac{1}{4\pi\bar{d}(\bar{E})}\sum_t \sum_{k=-\infty}^{\infty}{}' \sum_{t'} \sum_{k'=-\infty}^{\infty}{}' \frac{A(t,k)\,A^\star(t',k')}{\bar{p}} \times \frac{1}{\sqrt{2\pi}\Delta p\mu}\,e^{i[kl(t)-k'l(t')]\frac{\bar{l}}{\mu}}\,e^{-\frac{(\bar{l}/\mu-\bar{p})^2}{2\Delta p^2}} \quad , \tag{32}$$

with $\mu := 4\pi\bar{d}(\bar{E})\tau$ and $\bar{l} := \frac{1}{2}[kl(t)+k'l(t')]$.

Now we would like to discuss the so-called diagonal approximation of (32), which plays a central role in all explanations of the peculiar behavior of arithmetical quantum chaos. The diagonal approximation $K_{\rm sc}^D(\tau)$ consists of replacing the quadruple sum in (32) by the double sum over the diagonal elements $t = t'$ and $k = k'$, which should be justified for very small values of τ such that $K_{\rm sc}(\tau) \simeq K_{\rm sc}^D(\tau)$ in the range of validity. In the case of a chaotic system possessing only time-reversal symmetry without arithmetical properties, one has $K_{\rm sc}^D(\tau) = 2\tau$, which agrees with the small τ behavior of the GOE form factor $K_{\rm GOE}(\tau) \sim 2\tau$; see Eq. (43) below. In [5] it was demonstrated that this behavior arises from a constant multiplicity $g = 2$ of the periodic orbits and that for systems without time-reversal symmetry a constant multiplicity $g = 1$ leads to $K_{\rm sc}^D(\tau) = \tau$. For systems with arithmetical chaos one expects in contrast an exponentially increasing spectral form factor at least for

those small values of τ where the diagonal approximation is justified. This is the basis for the explanation of the special properties of arithmetical quantum chaos [12,15]. To derive the diagonal approximation in the arithmetical case, we replace $A(t,k)$ by its asymptotic value $A(t,k) \simeq [\chi(t)]^k l(t) e^{-kl(t)/2}$ and sum over distinct lengths, i.e., we take into account the mean degeneracy $\langle g(l) \rangle = c_\Gamma e^{l/2}/l$ and use $N_{\text{distinct}}(l) = \frac{2}{c_\Gamma} e^{l/2}$, which leads to

$$K_{\text{sc}}^D(\tau) = \frac{c_\Gamma}{4\pi \bar{d}(\bar{E})} \int_{l_0}^{\infty} dl\, e^{l/2} \frac{1}{\sqrt{2\pi}\Delta p} e^{-\frac{(l/\mu-\bar{p})^2}{2\Delta p^2}} , \tag{33}$$

where l_0 denotes the shortest length. This is the diagonal approximation for a finite energy averaging. To obtain the result in [12,15], the limit $\Delta p \to 0$ has to be considered, in which the Gaussian in the integral including its prefactor gives a δ function. This leads to

$$K_{\text{sc}}^D(\tau) = \frac{c_\Gamma}{4\pi \bar{d}(\bar{E})\bar{p}} e^{2\pi \bar{d}(\bar{E})\bar{p}\tau} . \tag{34}$$

In [12,15] it is assumed that the true spectral form factor shows for small τ exactly this exponential behavior until it reaches the saturation value 1 and thus one arrives at the following simplified model for the spectral form factor:

$$K_{\text{model}}(\tau) := \min\left(1, \frac{c_\Gamma}{4\pi \bar{d}(\bar{E})\bar{p}} e^{2\pi \bar{d}(\bar{E})\bar{p}\tau}\right) . \tag{35}$$

One sees that (35) reaches the value one at

$$\tau_d = \frac{1}{2\pi \bar{d}(\bar{E})\bar{p}} \ln\left(\frac{4\pi \bar{d}(\bar{E})\bar{p}}{c_\Gamma}\right) , \tag{36}$$

which is the maximal τ value up to which the diagonal approximation must be employed. With (27) one can predict the number variance using the model form factor (35) and the spectral rigidity using (14).

Let us now turn to the crucial question of whether the diagonal approximation is justified at all in the case of finite-energy averaging $\Delta p > 0$. Equation (32) shows that each term contributes a Gaussian $\exp[-(\bar{l}/\mu - \bar{p})^2/(2\Delta p^2)]$. Thus the diagonal approximation breaks down if the width of the Gaussian is comparable to the distance between neighboring Gaussians. Since we need the width of the Gaussian in τ, we Taylor expand the argument of the Gaussian having the form

$$\begin{aligned} &\exp\left[-\frac{1}{2\sigma^2}\left(\frac{1}{\tau} - \frac{1}{\tau_0}\right)^2\right] \\ &\simeq \exp\left(-\frac{1}{2\sigma^2\tau_0^4}(\tau - \tau_0)^2\right) \\ &=: \exp\left(-\frac{1}{2\Delta\tau^2}(\tau - \tau_0)^2\right), \end{aligned} \tag{37}$$

which is valid up to $O((\tau - \tau_0)^3)$. One concludes that the Gaussian has a width of approximately

$$\Delta\tau = \frac{\bar{l}\Delta p}{4\pi \bar{p}^2 \bar{d}(\bar{E})} , \tag{38}$$

which by means of (30) corresponds to a "length width" of $\Delta l = \frac{\Delta p}{\bar{p}} l$. Since the distance between neighboring lengths is approximately given by $\Delta l = c_\Gamma e^{-l/2}$, one obtains overlapping Gaussians at a length given by the transcendental equation

$$\hat{l}\, e^{\hat{l}/2} = c_\Gamma \frac{\bar{p}}{\Delta p} . \tag{39}$$

This determines the maximal length and with (30) the maximal τ value $\hat{\tau}$ at which the diagonal approximation is an appropriate description of the spectral form factor. To justify the model form factor (35), it is necessary that the diagonal approximation is valid up to τ_d, defined in (36). Thus, for a given energy averaging at $\bar{p}$ with width Δp, one must require $\tau_d < \hat{\tau}$. From condition (39) it follows that in the limit $\Delta p \to 0$ the diagonal approximation is valid for an increasing τ interval such that (35) is justified in this limit. However, the breakdown can be caused by a finite value of Δp as it is required for any application.

For a numerical evaluation of the spectral form factor $K(\tau)$ in terms of the quantal levels it is convenient to employ a semiclassical approximation that is obtained from (29) by a Gaussian averaging in p followed by an additional Gaussian averaging in τ yielding the relation [32,33]

$$\begin{aligned} K_{\text{sc}}(\tau) = \frac{\Delta p}{(2\pi)^{3/2}\bar{p}\,\bar{d}(\bar{E})} \Bigg| \sum_t {\sum_{k=-\infty}^{\infty}}' A(t,k) \\ \times \exp[i\bar{p}kl(t)] \exp\left(-\Delta p^2 \{\ell - k[l(t)]\}^2\right) \Bigg|^2 . \end{aligned} \tag{40}$$

Although formula (40) was originally derived to extract information from the periodic orbits, one can also reverse the point of view with the help of the trace formula (21). This is possible because the quadruple sum that naturally occurs in the periodic-orbit expression for $K_{\text{sc}}(\tau)$ is effectively reduced in Eq. (40) to a double periodic-orbit sum. (Note, however, that a quadruple sum is still present because of the modulus square.) An exact periodic-orbit expression for $K(\tau)$ has been derived in [34]. But since it is not possible to reduce the quadruple sum in this exact expression, one cannot evaluate the exact formula using the quantal levels via the trace formula (21). Thus we shall now use the semiclassical expression (40). To express the periodic-orbit sum in terms of the quantal levels we choose, in the trace formula,

$$\begin{aligned} h(p) = \frac{\sqrt{\pi}}{\Delta p}\Bigg\{ &\exp\left(-\frac{(p-\bar{p})^2}{4\Delta p^2} - i(p-\bar{p})\ell\right) \\ &+ \exp\left(-\frac{(p+\bar{p})^2}{4\Delta p^2} - i(p+\bar{p})\ell\right)\Bigg\}, \end{aligned} \tag{41}$$

whose Fourier transform reads

$$\begin{aligned} g(x) = &\exp[-\Delta p^2(\ell - x)^2 + i\bar{p}x] \\ &+ \exp[-\Delta p^2(\ell + x)^2 - i\bar{p}x] . \end{aligned} \tag{42}$$

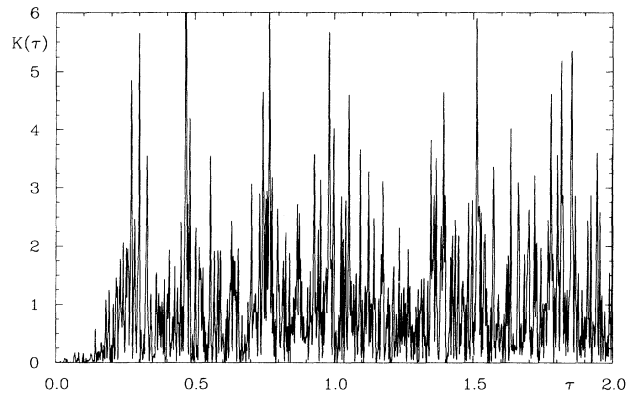

FIG. 11. The spectral form factor is shown for billiard $\mathcal{B}$ with the parameters $\overline{p} = 270$ and $\Delta p = 10$.

The Fourier transform (42) is exactly the expression that occurs in (40). Thus we can identify the periodic-orbit sum in Eq. (40) with the corresponding sum in the trace formula (21), which in turn allows us to replace the sum over periodic orbits by the left-hand side of the trace formula, i.e., by a sum over the quantal energies. In our numerical evaluation we subtract from the sum over the quantal levels the zero-length contribution, the sum over the inversion elements t_{inv}, and the sum over the elliptic elements t_{ellip}. Then only the periodic orbit sum is obtained. To justify this subtraction note that $d_{\mathrm{fl}}(E)$ occurs in Eq. (28). Since the zero-length term corresponds to the area term and part of the constant in Weyl's law, the sum over the inversion elements to the perimeter term, and the sum over the elliptic elements to the other part of the constant, one has indeed computed the contributions to $d_{\mathrm{fl}}(E)$.

The obtained spectral form factor is connected with the number variance defined by a Gaussian averaging at momentum $\overline{p}$ and width Δp (instead of the rectangular averaging used in Sec. III C). In the following two different energy ranges are studied: a low-energy range defined by $\overline{p} = 150$, $\Delta p = 15$ and a high-energy range defined by $\overline{p} = 270$, $\Delta p = 10$. The spectral form factor is a rapidly fluctuating function. As an example Fig. 11 presents the spectral form factor for billiard $\mathcal{B}$ at $\overline{p} = 270$. The strong fluctuations are not an artifice of the employed approximations since this behavior has also been observed for the exact spectral form factor [34]. Because the strong fluctuations hide the mean properties, we average the spectral form factor such that the wildest fluctuations are suppressed. The result is shown in Fig. 12 for the

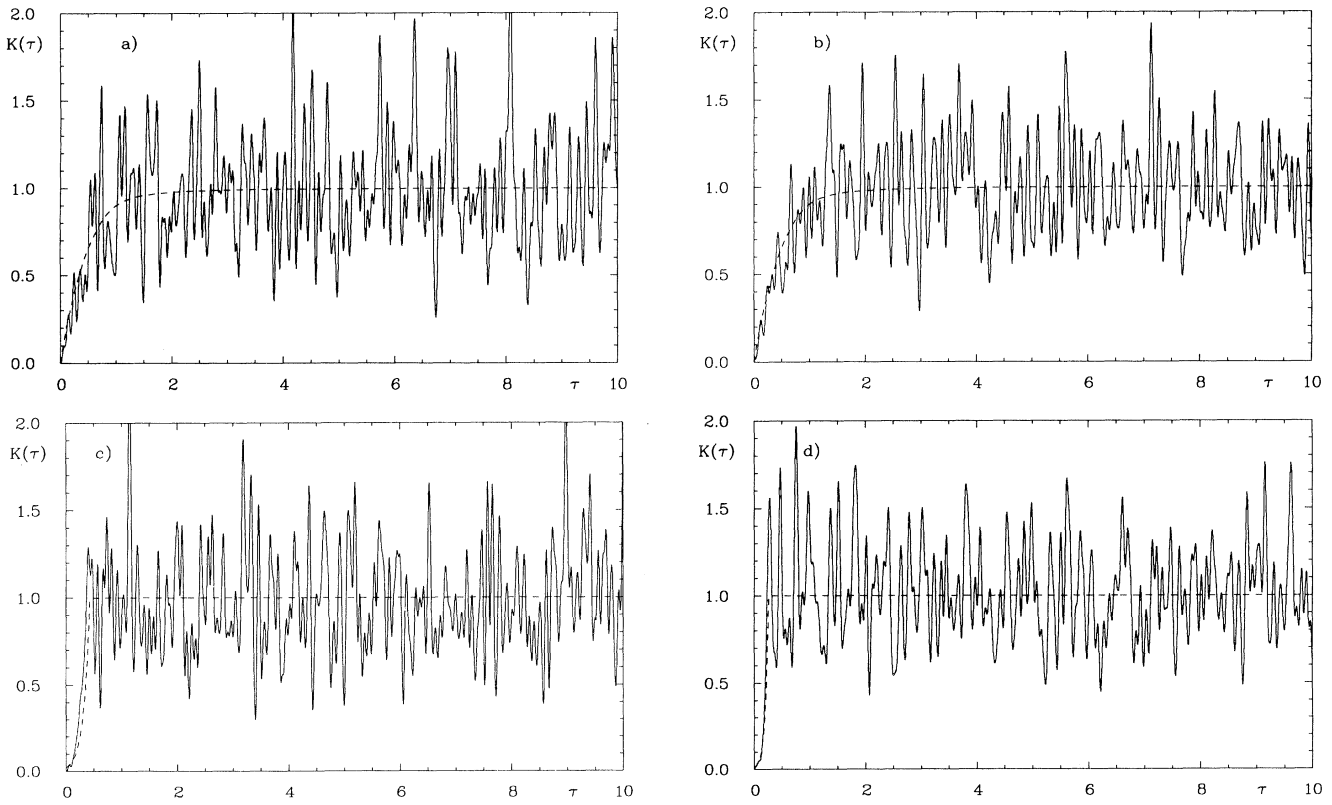

FIG. 12. The smoothed spectral form factor is shown for billiard $\mathcal{A}$ in (a) $(\overline{p} = 150, \Delta p = 15)$ and (b) $(\overline{p} = 270, \Delta p = 10)$ in comparison with the GOE spectral form factor (43) (dashed curve). (c) $(\overline{p} = 150, \Delta p = 15)$ and (d) $(\overline{p} = 270, \Delta p = 10)$ display the smoothed spectral form factor for billiard $\mathcal{B}$ in comparison with the exponential model form factor (35) (dashed curve) discussed in the text.

two billiards in the low- and in the high-energy range. In all four cases the spectral form factor saturates for $\tau > 1$ and fluctuates around the value one, which exemplifies the fact that formula (40) deals in fact with a quadruple sum, i.e., it includes nondiagonal contributions since it would otherwise display the behavior of the diagonal approximation that always increases with τ. The GOE spectral form factor

$$K_{\mathrm{GOE}}(\tau) = \begin{cases} 2\tau - \tau\ln(1+2\tau) & , \ 0 \le \tau \le 1 \\ 2 - \tau\ln\left(\frac{2\tau+1}{2\tau-1}\right) & , \ \tau \ge 1 \end{cases} \tag{43}$$

is also shown in Figs. 12(a) and 12(b) dealing with billiard $\mathcal{A}$. Despite the fluctuations, rough agreement is observed. This also demonstrates the stationarity of the level fluctuations for billiard $\mathcal{A}$.

A completely different behavior is revealed for $\tau < 1$ for billiard $\mathcal{B}$ where the spectral form factor increases in general much faster than the GOE behavior. In Figs. 12(c) and 12(d) the model form factor (35) is shown where the value $c_\Gamma = \frac{1}{1+\sqrt{2}}$ is used. Surprisingly good agreement with the mean behavior of the spectral form factor is observed. Note, however, that the same model spectral form factor should also describe billiard $\mathcal{A}$. There remains the question of why this argumentation leads to a satisfactory description for billiard $\mathcal{B}$ and not for billiard $\mathcal{A}$ having the same multiplicities. Using Eq. (39) one obtains for $\bar{p} = 150$ and $\Delta p = 15$ the value $\widehat{\tau} = 0.0885$, up to which the diagonal approximation is justified, whereas in the case of the model form factor the diagonal approximation is employed up to $\tau_d = 0.393$. This shows that the diagonal approximation is not valid over practically the whole τ interval. The inapplicability of the model form factor is even more obvious if one notes that $K_{\mathrm{sc}}^D(\widehat{\tau}) \simeq 0.050$, whereas the GOE form factor is at the same $\widehat{\tau}$ value already as large as $K_{\mathrm{GOE}}(\widehat{\tau}) \simeq 0.177$. Here arises the odd situation that the diagonal approximation of the form factor, which should explain by its fast increasing behavior the peculiar spectral statistics, is actually smaller than the GOE form factor. One faces a similar situation in the higher-energy range, i.e., for $\bar{p} = 270$ and $\Delta p = 10$, where one gets $\widehat{\tau} = 0.0787$ and $\tau_d = 0.256$ together with $K_{\mathrm{sc}}^D(\widehat{\tau}) \simeq 0.047$ and $K_{\mathrm{GOE}}(\widehat{\tau}) \simeq 0.157$. One thus concludes that the diagonal approximation is not valid in both cases. Nevertheless, it is very strange to observe in Figs. 12(c) and 12(d) much better agreement with the model form factor than with the GOE form factor, which is in contrast to Figs. 12(a) and 12(b), which

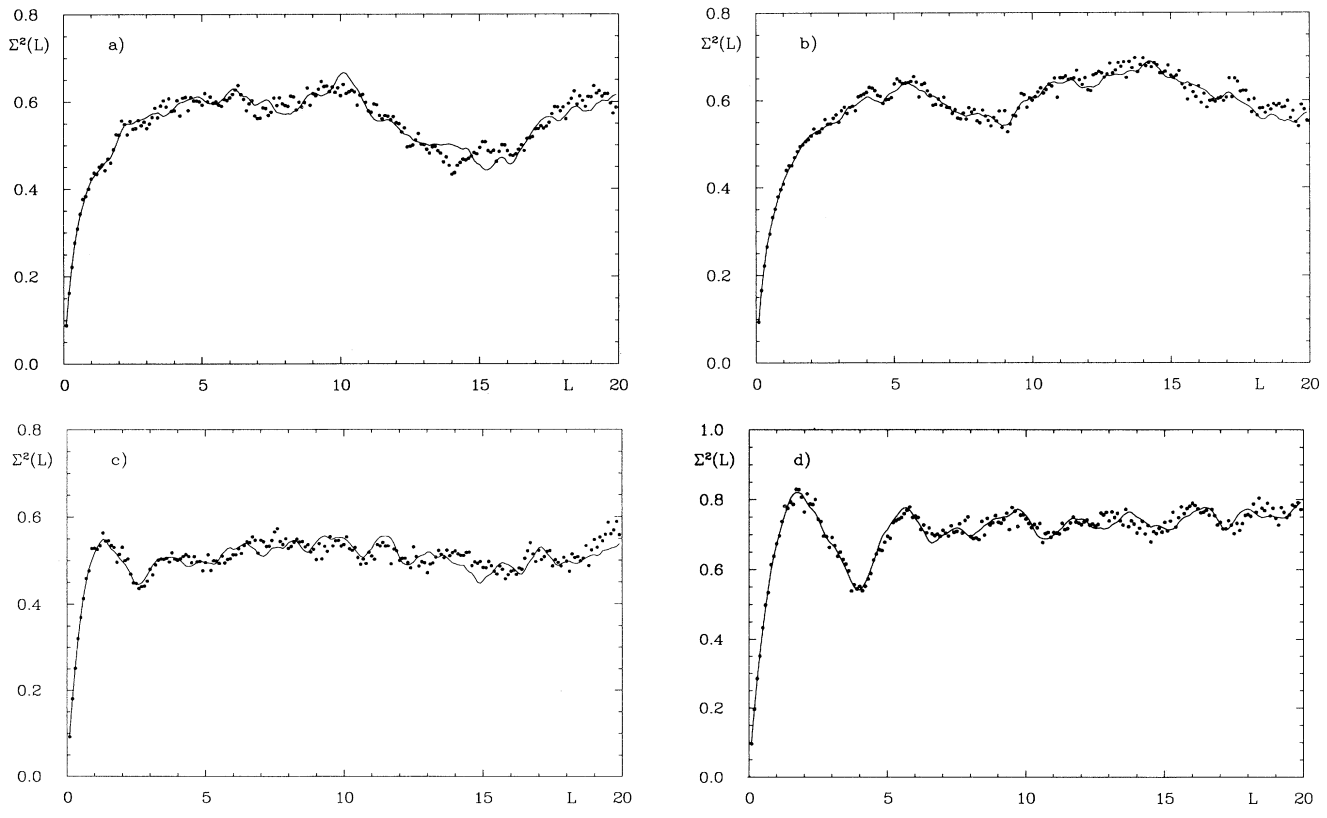

FIG. 13. The number variance $\Sigma^2(L)$ is shown for billiard $\mathcal{A}$ in (a) ($\bar{p} = 150, \Delta p = 15$) and (b) ($\bar{p} = 270, \Delta p = 10$). The full curve is obtained from the approximate spectral form factor (40) using the integral representation (27), whereas the dots are obtained directly from the quantal spectrum using 5000 sample points. (c) ($\bar{p} = 150, \Delta p = 15$) and (d) ($\bar{p} = 270, \Delta p = 10$) display the same quantities for billiard $\mathcal{B}$.

show good agreement with the GOE form factor. Since the model form factor is neither applicable nor able to explain the differences in the energy spectra of the two billiards, there must be another origin of the differences. One possibility could be a strange correlation between the characters of neighboring orbits in such a way that the different spectral form factors are generated, where, however, the contributions of nondiagonal elements must play a significant role.

Since the spectral form factor (40) is based on a semiclassical approximation, it is important to check also the validity of (40) at least numerically. To this aim we computed the number variance $\Sigma^2(L)$ using the spectral form factor (40) in the integral equation (27). The results are compared with the "true" number variance, which is obtained by averaging the number variance of the quantal levels at 5000 random sample points p, which in turn are Gaussian distributed according to $\overline{p}$ and Δp. The results shown in Fig. 13 demonstrate that the approximation is at least numerically justified.

V. SUMMARY AND DISCUSSION

We have studied the level statistics of two strongly chaotic quantum billiards. Since the billiard ball table was for both billiards the same non-Euclidean triangle, the two billiards are classically identical in that they possess the same classical periodic orbits. They only differ in the boundary conditions imposed on the quantum mechanical wave functions, which is reflected in different characters, i.e., in different signs of the amplitudes attached to the periodic orbits in the trace formula. For the triangular billiard domain we have chosen the fundamental domain of the reflection group $\mathrm{T}^*(2,3,8)$. Since this group is an arithmetical group, the periodic orbits possess an exponentially degenerate length spectrum. The boundary conditions have been chosen in such a way that billiard $\mathcal{A}$ does not belong to a representation of the reflection group, whereas the boundary conditions imposed on billiard $\mathcal{B}$ are compatible with an irreducible symmetry representation.

A previous analysis [17] based on the first 200 energy levels revealed for billiard $\mathcal{B}$ the peculiar level statistics characteristic for arithmetical quantum chaos. It turned out, however, that the level statistics of billiard $\mathcal{A}$ are at short- and medium-range correlations in accordance with the GOE behavior of random-matrix theory typically found for generic systems. There remained the important question of whether this mysterious difference between these almost identical billiards is only a low-energy effect or whether it could be confirmed over a much larger energy range and with much better statistics.

In this paper we have extended the previous analysis using now for both billiards the first 1050 levels, which we have computed using the boundary element method. Our analysis covers the full energy range up to $E = 100\,000$. In Sec. III we presented a detailed analysis of the level statistics that shows clearly that billiard $\mathcal{A}$ indeed behaves like a generic chaotic quantum system, while billiard $\mathcal{B}$ shows the typical behavior of arithmetical quantum chaos.

Since the level statistics of quantum billiard $\mathcal{A}$ show all properties of generic quantum chaos, although the classical counterpart possesses the strange arithmetical structure typical for arithmetical chaos, we call this dynamical system *pseudoarithmetical* in order to distinguish it from systems such as quantum billiard $\mathcal{B}$, which is a genuine *arithmetical* system, showing the exceptional level statistics characteristic for arithmetical quantum chaos.

The number variance $\Sigma^2(L)$ and the spectral rigidity $\Delta_3(L)$ show for both billiards a saturation plateau at long-range correlations and thus a breakdown of the universal behavior derived for random matrices. Of special interest is the energy dependence of the plateau height $\Delta_\infty(E)$, which we have computed in Sec. III D. As expected, we find that the energy dependence of $\Delta_\infty(E)$ is, for the pseudoarithmetical billiard $\mathcal{A}$, in good agreement with a logarithmic increase (see Fig. 7), in accordance with Berry's semiclassical analysis [5] for generic chaotic systems being invariant under time reversal. It turns out, however, that a fit of the form $\Delta_\infty(E) = \frac{1}{2\pi^2}\ln E + \gamma$, shown as the full curve in Fig. 7, gives, for the constant γ, a value that does not agree with the constant $c(l_0)$ in Berry's formula (15) that is solely determined by the length l_0 of the shortest periodic orbit. This agrees with an earlier analysis [34] that already showed that the precise saturation value is determined by the lower part of the length spectrum of periodic orbits, but not just by the very shortest orbit. In the case of the arithmetical billiard $\mathcal{B}$ we find that the energy dependence agrees well with the simple ansatz $\Delta_\infty(E) = \alpha\sqrt{E} + \beta$ (see the dotted curve in Fig. 7), which generically holds for integrable systems. In [12] a $\sqrt{E}/\ln E$ behavior was derived from a simple model of arithmetical quantum chaos, a behavior that is, however, excluded by our data. This gives a first hint that there are subtle properties of arithmetical systems that require a modification of the simple model proposed in [12].

Knowing the correct energy dependence of $\Delta_\infty(E)$ gave us the opportunity to calculate the value distribution $P(W)$ of the mode fluctuation $W(E)$ defined in Eq. (17). According to a recent conjecture [21,22], $P(W)$ should display, for both billiards in the semiclassical limit, the parameter-free universal Gaussian behavior (20). The comparison presented in Figs. 8(a) and 8(b) gives strong support to this conjecture. The important point is that the distribution $P(W)$ gives us a universal measure for quantum chaos that depends only on whether the corresponding classical system is strongly chaotic or not, independent of whether the system is arithmetical, pseudoarithmetical, or generic.

In Sec. IV we employed the periodic-orbit theory to shed some light on the observed level statistics for billiards $\mathcal{A}$ and $\mathcal{B}$. In the case of the arithmetical quantum billiard $\mathcal{B}$, one has the exact Selberg trace formula (21) recently derived in [25], whereas for the pseudoarithmetical quantum billiard $\mathcal{A}$, one has to rely on Gutzwiller's semiclassical trace formula [2] appropriately generalized to the non-Euclidean geometry of billiard $\mathcal{A}$. In our analysis carried out in Sec. IV we assumed that the trace formula for the pseudoarithmetical system was again given

by Eq. (21), but that in this case it was only semiclassically valid, i.e., we assumed that the unknown correction terms, which have to be added to the right-hand side of Eq. (21), were subdominant in the semiclassical limit and thus did not alter the main results of our analysis.

Using the computed quantal levels up to $E = 100\,000$, we computed in Sec. IV B the truncated trace of the cosine-modulated heat kernel $\Theta^C(L)$ [see Eq. (26)] for fixed $\beta = 0.000\,05$ as a function of L. The idea, of course, was that this function would exhibit a different behavior depending on the arithmetical and pseudoarithmetical case, respectively. Since $\Theta^C(L)$ has an alternative representation, derived from the right-hand side of the trace formula, as a sum over periodic orbits, it could be expected that the different behavior seen in the level statistics would find its correspondence in a different behavior of the function $\Theta^C(L)$ for the two billiards. The results presented in Figs. 9 and 10 show, however, that billiard $\mathcal{A}$ and $\mathcal{B}$ behave in a very similar way.

To settle the question concerning the characters, we investigated in Sec. IV C the semiclassical spectral form factor $K_{\rm sc}(\tau)$ defined in Eq. (28). (For a critical discussion of this approximation, we refer to [34].) Since the expression (28) does not allow a meaningful computation using the known energy levels, we employed a further approximation leading to the expression (40), which can now be completely expressed in terms of the energy levels using the test function (41) in the trace formula. Using this formula we obtained, for the form factor, the results shown in Figs. 11 and 12. Figure 11 shows that the form factor is a very spiky function, and we have shown in Figs. 12(a)–12(d) a smoothed version where the wildest fluctuations have been suppressed. Figures 12(a) and 12(b) show that the mean behavior of the smoothed form factor for the pseudoarithmetical billiard $\mathcal{A}$ is in good overall agreement with the GOE form factor and thus in conformity with the generic level statistics that we have found for this billiard. In contrast, the mean behavior of the smoothed form factor for the arithmetical billiard $\mathcal{B}$, represented in Figs. 12(c) and 12(d), is in good overall agreement with the model form factor (35) whose derivation made essential use of the exponential multiplicity of the periodic orbits. Thus the spectral form factor behaves very differently for the two billiards in accordance with the different level statistics observed for billiards $\mathcal{A}$ and $\mathcal{B}$. This proves that the spectral form factor is a sensitive measure for the delicate differences between the two almost identical billiards. In particular, it demonstrates that the main difference between arithmetical and pseudoarithmetical quantum chaos is caused by subtle properties of the characters attached to the classical periodic orbits and/or by the nonperiodic orbit contributions, which are not taken into account in our trace formula.

It is worthwhile to mention that the observation that the characters attached to the periodic orbits show, for arithmetical systems, a different behavior than for generic ones has already been made in a previous paper [35]. There it was shown that the signs of the coefficients of the Dirichlet series expansion of the dynamical ζ function behave completely differently in the case of Artin's billiard, which is arithmetical, compared to generic systems. (The signs of the Dirichlet coefficients are directly related to the characters.)

Future progress towards a deeper understanding of the subtleties of arithmetical and pseudoarithmetical quantum chaos may be achieved in the following three steps. In the first step one has to justify the approximate representation (40) for the spectral form factor, which yields numerically reasonable results, as we have demonstrated in Fig. 13. In the second step one has to incorporate the properties of the length spectrum of periodic and nonperiodic orbits and, very importantly, the subtle behavior of the characters attached to them. Finally, in the third step, one has to extract from formula (40) the mean behavior of the spectral form factor. As a result one would obtain an improved model for the form factor that would include nondiagonal contributions, which are very essential as we have emphasized in Sec. IV C. From the improved form factor one could then compute the various level statistics. We hope to return to these points in a future paper.

ACKNOWLEDGMENTS

It is a pleasure to thank H. Ninnemann for helpful discussions. Furthermore, we would like to thank the Deutsche Forschungsgemeinschaft for financial support under Contracts Nos. DFG-Ste 241/4-6 and DFG-Ste 241/6-1.

[1] M. L. Mehta, *Random Matrices and the Statistical Theory of Energy Levels*, new revised and enlarged edition (Academic, New York, 1990).
[2] M. C. Gutzwiller, *Chaos in Classical and Quantum Mechanics* (Springer, New York, 1990).
[3] O. Bohigas, M.-J. Giannoni, and C. Schmit, Phys. Rev. Lett. **52**, 1 (1984).
[4] O. Bohigas, M.-J. Giannoni, and C. Schmit, J. Phys. (Paris) Lett. **45**, L1015 (1984).
[5] M. V. Berry, Proc. R. Soc. London Ser. A **400**, 229 (1985).
[6] O. Bohigas, M.-J. Giannoni, and C. Schmit, in *Spectral Fluctuations, Random Matrix Theories and Chaotic Motion*, edited by Editor(s), Lecture Notes in Physics Vol. 262 (Springer, Heidelberg, 1986).
[7] R. Aurich and F. Steiner, Physica D **43**, 155 (1990).
[8] N. L. Balazs and A. Voros, Phys. Rep. **143**, 109 (1986).
[9] R. Aurich and F. Steiner, Physica D **32**, 451 (1988).
[10] R. Aurich, E. B. Bogomolny, and F. Steiner, Physica D **48**, 91 (1991).
[11] J. Bolte, Nonlinearity **6**, 935 (1993).
[12] J. Bolte, Int. J. Mod. Phys. B **7**, 4451 (1993).
[13] C. Matthies and F. Steiner, Phys. Rev. A **44**, R7877 (1991).

[14] J. Bolte, G. Steil, and F. Steiner, Phys. Rev. Lett. **69**, 2188 (1992).
[15] E. B. Bogomolny, B. Georgeot, M.-J. Giannoni, and C. Schmit, Phys. Rev. Lett. **69**, 1477 (1992).
[16] G. Steil, DESY Report No. DESY 94-028, 1994 (unpublished).
[17] R. Aurich, Ph.D. thesis, Universität Hamburg, 1990.
[18] A. Selberg, J. Indian Math. Soc. **20**, 47 (1956).
[19] R. Aurich and F. Steiner, Physica D **64**, 185 (1993).
[20] F. J. Dyson and M. L. Mehta, J. Math. Phys. **4**, 701 (1963).
[21] F. Steiner, in *Schlaglichter der Forschung. Zum 75. Jahrestag der Universität Hamburg 1994*, edited by R. Ansorge (Reimer, Berlin, 1994), p. 543.
[22] R. Aurich, J. Bolte, and F. Steiner, Phys. Rev. Lett. **73**, 1356 (1994).
[23] D. R. Heath-Brown, Acta Arithmetica **60**, 389 (1992); P. M. Bleher, Z. Cheng, F. J. Dyson, and J. L. Lebowitz, Commun. Math. Phys. **154**, 433 (1993); P. M. Bleher, D. V. Kosygin, and Y. G. Sinai, Princeton University Report (unpublished).
[24] A. Selberg, Arch. Math. Naturvid. B **48**, 89 (1946); A. Ghosh, J. Number Theory **17**, 93 (1983); H. L. Montgomery, in *Number Theory, Trace Formulas and Discrete Groups*, edited by K. E. Aubert, E. Bombieri, and D. Goldfeld (Academic, New York, 1989), p. 157.
[25] H. Ninnemann, Ph.D. thesis, Universität Hamburg, 1994; DESY Report No. DESY 94-241, 1994 (unpublished).
[26] M. Sieber and F. Steiner, Phys. Lett. A **144**, 159 (1990).
[27] R. Aurich, C. Matthies, M. Sieber, and F. Steiner, Phys. Rev. Lett. **68**, 1629 (1992).
[28] R. Aurich, M. Sieber, and F. Steiner, Phys. Rev. Lett. **61**, 483 (1988).
[29] R. Aurich and F. Steiner, Physica D **39**, 169 (1989).
[30] R. Aurich and F. Steiner, Phys. Rev. A **45**, 583 (1992).
[31] F. J. Dyson, J. Math. Phys. **3**, 166 (1962).
[32] N. Argaman, Y. Imry, and U. Smilansky, Phys. Rev. B **47**, 4440 (1993).
[33] R. Aurich and M. Sieber, J. Phys. A **27**, 1967 (1994).
[34] R. Aurich and F. Steiner, DESY Report No. DESY 94-058, 1994 (unpublished); Physica D (to be published).
[35] R. Aurich, J. Bolte, C. Matthies, M. Sieber, and F. Steiner, Physica D **63**, 71 (1993).